Block Sparse Bayesian Learning-Based NB-IoT Interference Elimination in LTE-Advanced Systems

Sicong Liu, *Student Member, IEEE*, Fang Yang, *Senior Member, IEEE*, Jian Song, *Fellow, IEEE*, and Zhu Han, *Fellow, IEEE*

***Abstract*— Narrowband Internet-of-Things (NB-IoT) is one of the emerging 5G technologies, but might introduce narrowband interference (NBI) to existing broadband systems, such as long-term evolution advanced (LTE-A) systems. Thus, the mitigation of the NB-IoT interference to LTE-A is an important issue for the harmonic coexistence and compatibility between 4G and 5G. In this paper, a newly emerged sparse approximation technique, block sparse Bayesian learning (BSBL), is utilized to estimate the NB-IoT interference in LTE-A systems. The block sparse representation of the NBI is constituted through the proposed temporal differential measuring approach, and the BSBL theory is utilized to recover the practical block sparse NBI. A BSBL-based method, partition estimated BSBL, is proposed. With the aid of the estimated block partition beforehand, the Bayesian parameters are obtained to yield the NBI estimation. The intra-block correlation (IBC) is considered to facilitate the recovery. Moreover, exploiting the inherent structure of the identical IBC matrix, another method of informative BSBL is proposed to further improve the accuracy, which does not require prior estimation of the block partition. Reported simulation results demonstrate that the proposed methods are effective in canceling the NB-IoT interference in LTE-A systems, and significantly outperform other conventional methods.**

***Index Terms*— Narrowband Internet-of-Things, long term evolution advanced, narrowband interference, block sparse Bayesian learning, temporal differential measuring.**

Manuscript received January 9, 2017; revised May 24, 2017; accepted June 28, 2017. Date of publication July 5, 2017; date of current version October 16, 2017. This work was supported by the Shenzhen International Cooperation Project (Grant No. GJHZ20160301092608343), National Key Research and Development Program (Grant No 2017YFB0403402), National Natural Science Foundation of China (Grant No. 61401248), New Generation Broadband Wireless Mobile Communication Network of the National Science and Technology Major Projects (Grant No. 2015ZX03002008), Young Elite Scientist Sponsorship Program by CAST (Grant No. YESS20150120), US NSF CNS-1702850, CNS-1646607, ECCS-1547201, CCF-1456921, CMMI-1434789, CNS-1443917, and ECCS-1405121. The associate editor coordinating the review of this paper and approving it for publication was M. Di Renzo. *(Corresponding author: Fang Yang.)*

S. Liu is with the Tsinghua National Laboratory for Information Science and Technology, Electronic Engineering Department, Research Institute of Information Technology, Tsinghua University, Beijing 100084, China (e-mail: liu-sc12@mails.tsinghua.edu.cn).

F. Yang and J. Song are with the Tsinghua National Laboratory for Information Science and Technology, Electronic Engineering Department, Research Institute of Information Technology, Tsinghua University, Beijing 100084, China, and also with the Key Laboratory of Digital TV System of Guangdong Province and Shenzhen City, Shenzhen 518057, China (e-mail: fangyang@tsinghua.edu.cn; jsong@tsinghua.edu.cn).

Z. Han is with the Department of Electrical and Computer Engineering, University of Houston, Houston, TX 77204-4005 USA (e-mail: zhan2@uh.edu).

Color versions of one or more of the figures in this paper are available online at http://ieeexplore.ieee.org.

Digital Object Identifier 10.1109/TCOMM.2017.2723572

I. Introduction

LONG term evolution advanced (LTE-A) radio access network (RAN) and technologies have been drawing a lot of attention from both industry and academia, boldly paving the way from 4G to 5G technologies [1], [2]. Cyclic-prefixed orthogonal frequency division multiplexing (CP-OFDM) plays an important role in RAN techniques of LTE-A due to its superior anti-frequency-selectivity capability and spectral efficiency, and thus also applied in many other broadband systems such as wireless local access networks (WLAN) [3]. Since there are a lot of different narrowband communications services occupying the same band adopted by the broadband LTE-A system, it is much likely for LTE-A base-stations (BS) or user equipment (UE) to suffer from narrowband interference (NBI) [4]. In LTE-A systems, NBI can be generated from lots of different sources. A major source is the narrowband internet-of-things (NB-IoT) system with "in-band" mode occupying some sub-bands out of the LTE-A band [5], which is much likely to interfere with and degrade the performance of the LTE-A systems [6]. As an ultra-low complexity and low power consumption technology with large coverage, NB-IoT is becoming a popular emerging technology in the area of IoT and machine-type communications, which is a competitive candidate for the 5G new radio scenarios and technologies [7]. When NB-IoT uses the same in-band resource already occupied by LTE-A, it is difficult for LTE-A systems to avoid the interference from NB-IoT without degradation of system performance and spectral efficiency. Hence, it is crucial to find solutions for the compatibility between NB-IoT and LTE-A to achieve smooth 4G/5G transition and harmonious coexistence between them, while maintaining the spectral efficiency of LTE-A systems.

The NBI generated by NB-IoT can be modeled as a sparse vector in the frequency domain, which has only few nonzero entries compared with the number of sub-carriers. More generally, the nonzero entries of the NBI are not necessarily located exactly at the frequencies of the sub-carriers in practical OFDM-based systems. Namely, there might be a fractional frequency offset (FO) with respect to the OFDM sub-carriers, so the NBI will be a block sparse vector due to the spectral leakage [8], i.e., the nonzero entries are clustered in blocks.

Conventional methods include the frequency threshold excision (FTE) approach [9] that excludes the NBI contaminated sub-carriers, the linear minimum mean square error estimation method [10], and the successive cancellation method [11], the spectral shaping NBI avoidance method [12], the constrained maximum-signal-to-interference-noise-ratio equalizer method [13], etc. Nevertheless, these conventional methods process with the NBI by only excluding or suppressing its power, but not reconstructing the exact NBI signal and cancelling it from the data, so the impact of NBI cannot be comprehensively eliminated. Hence, advanced physical layer techniques are necessarily essential to improve the robustness of broadband transmission systems against NBI.

Recently, the compressed sensing (CS) theory [14] is applied in NBI estimation [15]–[19]. Al-Dhahir *et al* first applied CS principle in NBI estimation for OFDM systems, and extended to power line communication and relay systems for the NBI with frequency offset [15]–[17]. Another method was proposed using training sequence to estimate NBI based on CS in literature [18], [19]. However, the CS-based NBI mitigation method exploiting the training sequence in time-domain synchronous OFDM (TDS-OFDM) systems [18] is not designed for cyclic prefixed OFDM (CP-OFDM). The NBI estimated from the preamble [19] might turn out inaccurate for the payload data symbols since it is not adaptively updated for each payload OFDM symbol. In addition, CS methods tend to suffer from large sparsity levels of the block sparse NBI in practice.

Another newly emerging and powerful theory for sparse approximation, block sparse Bayesian learning (BSBL), is proposed to utilize the intra-block correlation (IBC) to recover block sparse signals to achieve superior performance than CS methods, such as the BSBL-expectation maximization (BSBL-EM) algorithm [20]. The block sparse nature of the NBI with FO inspires us to exploit BSBL for NBI recovery to solve the problems of both conventional and CS based methods. By iteratively learning the unknown statistical parameters of the NBI based on a sparse Bayesian learning regime, the BSBL based algorithms are capable of deriving a more accurate posterior estimation of the NBI than CS and conventional methods. Based on the comprehensive literature survey on the related topics, there is no existing research of NBI recovery based on BSBL, and no state-of-art research that has considered the IBC within the blocks of the block sparse NBI to facilitate the NBI estimation. The prosperity of the BSBL theory in sparse signal processing in literature motivates us to exploit the IBC and introduce the BSBL theory to the NBI recovery to fill this gap.

Hence, to solve the problems of the NB-IoT interference estimation and cancelation in LTE-A systems, the BSBL theory based approach of NBI cancellation is proposed in this paper, which is the first BSBL based method in the area of NBI mitigation. Furthermore, the IBC of the NBI is also considered to facilitate the learning process and improve the performance of NBI reconstruction. The main contributions are as follows:

- To solve the difficulty in measuring the NBI mixed with the information data, a simple and effective temporal differential measuring (TDM) approach is proposed to establish the block sparse representations of the NBI, which is simply implemented by a differential operation between the CP and its duplex in the subsequent OFDM block.
- A BSBL based method, i.e., partition estimated BSBL (PE-BSBL), is proposed for NBI recovery. PE-BSBL first estimates the block partition by power thresholding, and then recover the NBI using expectation maximization (EM) [20], which significantly outperforms conventional methods.
- To further improve the performance, the informative BSBL (I-BSBL) method is proposed, which makes full use of the fact that IBC matrix is the same due to the same FO for different blocks. The IBC matrix is calculated beforehand without requiring the estimation of the block partition. Then an artificial non-overlapping block-sparse representation of the NBI is built up, based on which the NBI is recovered by the I-BSBL learning process to achieve better accuracy.

The advantages and the criterion of choosing a better algorithm from the two proposed algorithms are summarized as follows: 1) Whether the FO is known to the receiver or whether it can be well estimated. If the FO is known to the receiver or can be well estimated at the receiver, then I-BSBL is preferred, otherwise PE-BSBL is a relatively better choice. When the FO is well known or estimated, the prior information required by I-BSBL is more accurate. When the FO is not available, PE-BSBL is still capable of estimating the block partition. 2) Whether the FOs of all the NBI tone interferers are the same. If they are the same, then I-BSBL is preferred, otherwise PE-BSBL is better. The same FO is a basic assumption of I-BSBL. When the FOs are different from each other, PE-BSBL is still capable of estimating the block partition. 3) I-BSBL is proposed in the extended equivalent block-sparse framework of BLSBL, which is suited for the case where the block partition is completely unknown at the receiver. Although PE-BSBL does not require the block partition to be known, the block partition has to be estimated before iterations. Hence, in certain case that the block partition cannot be estimated accurately, the I-BSBL algorithm is more applicable.

The rest of this paper is organized as follows: Section II gives a brief review of the BSBL theory, and the system model is presented in Section III. The main contribution of this paper, the BSBL based sparse approximation method for NBI elimination in CP-OFDM incorporated LTE-A systems, is described in detail in Section IV, and the performance is evaluated through computer simulations in Section V, which is followed by the conclusions in Section VI. An initial conference version of part of this work is given in [21].

Notation: Matrices and column vectors are denoted by boldface letters; frequency-domain and time-domain vectors are denoted by boldface vectors with tilde $\tilde{\mathbf{v}}$ and without tilde $\mathbf{v}$, respectively; $(\cdot)^{\dagger}$ and $(\cdot)^{H}$ denote the pseudo-inversion operation and conjugate transpose, respectively; $\|\cdot\|_r$ represents the ℓ_r norm operation; $|\boldsymbol{\Omega}|$ denotes the cardinality of the set $\boldsymbol{\Omega}$; $\mathbf{v}|_{\boldsymbol{\Omega}}$ denotes the entries of the vector $\mathbf{v}$ in the set of $\boldsymbol{\Omega}$; $\mathbf{A}_{\boldsymbol{\Omega}}$ represents the sub-matrix comprised of the $\boldsymbol{\Omega}$ columns of the matrix $\mathbf{A}$; $\boldsymbol{\Omega}^c$ denotes the complementary set of $\boldsymbol{\Omega}$; $\mathrm{Max}(\mathbf{v}, T)$ denotes the indices of the T largest entries of the vector $\mathbf{v}$; $\mathbf{F}_N$ denotes the $N \times N$ inverse discrete Fourier transform (IDFT) matrix with the entry $\{\mathbf{F}_N\}_{m,n} = \exp\ (j2\pi mn/N)/\sqrt{N}$, and

$\mathbf{S}_{M,N}$ denotes the selection matrix composed of the last M rows of the $N \times N$ identity matrix $\mathbf{I}_N$ $(M < N)$. This way, the last M rows of $\mathbf{F}_N$ is denoted by $\mathbf{S}_{M,N}\mathbf{F}_N$.

II. A Brief Review of Block Sparse Bayesian Learning

In the BSBL framework [20], the goal is to reconstruct the *block sparse* vector $\mathbf{x}$ from a noisy measurement vector $\mathbf{y} \in \mathbb{C}^M$ $(M < N)$ given by

$$\mathbf{y} = \Phi\mathbf{x} + \mathbf{w}, \tag{1}$$

where Φ is the $M \times N$ observation matrix, $\mathbf{w}$ is a bounded background noise vector, and $\mathbf{x}$ is represented in a block sparse way given by

$$\mathbf{x} = [\underbrace{x_1, \cdots x_{d_1}}_{\mathbf{x}_1^T}, \cdots \underbrace{x_{d_{g-1}+1}, \cdots x_{d_g}}_{\mathbf{x}_g^T}]^T, \tag{2}$$

where the size of each block d_i is not necessarily identical. Only K_b $(K_b \ll g)$ blocks are nonzero among all the g blocks. Equation (1) is the block sparse representation of the NBI. In the BSBL framework, each block $\mathbf{x}_i \in \mathbb{C}^{d_i}$ is assumed to follow a parametric multivariate Gaussian distribution

$$p(\mathbf{x}_i; \gamma_i, \mathbf{B}_i) \sim \mathcal{N}(\mathbf{0}, \gamma_i\mathbf{B}_i), \quad i = 1, \cdots, g, \tag{3}$$

where the parameters $\mathbf{B}_i$ and γ_i are unknown to be determined. The block sparsity of $\mathbf{x}$ is determined by the nonnegative parameter γ_i, and nonzero γ_i indicates that the i-th block is nonzero. During the Bayesian learning procedure, most $\{\gamma_i\}_i$ asymptotically approach zero due to the automatic relevance determination mechanism, resulting in the block sparsity [20]. The IBC matrix is denoted by $\mathbf{B}_i \in \mathbb{C}^{d_i \times d_i}$, which is a positive definite matrix indicating the correlation structure within the i-th block. The IBC matrix $\mathbf{B}_i$ can be initialized by the covariance matrix, and it can be updated and optimized by the learning rules in the BSBL iterations. Under the assumption that blocks are mutually uncorrelated, the prior of $\mathbf{x}$ is $p(\mathbf{x}; \{\gamma_i, \mathbf{B}_i\}_i) \sim \mathcal{N}(\mathbf{0}, \Sigma_0)$, where the prior covariance matrix of $\mathbf{x}$ is given by

$$\Sigma_0 = \mathrm{diag}\{\gamma_1\mathbf{B}_1, \cdots, \gamma_g\mathbf{B}_g\}. \tag{4}$$

Assume that the noise follows the distribution $p(\mathbf{w}; \varepsilon) \sim \mathcal{N}(\mathbf{0}, \varepsilon\mathbf{I})$, where ε is the noise variance. The posterior of $\mathbf{x}$ is then derived as

$$p(\mathbf{x}|\mathbf{y}; \varepsilon, \{\gamma_i, \mathbf{B}_i\}_{i=1}^g) = \mathcal{N}(\boldsymbol{\mu}_x, \Sigma_x), \tag{5}$$

where

$$\boldsymbol{\mu}_x = \Sigma_0\Phi^T\left(\varepsilon\mathbf{I} + \Phi\Sigma_0\Phi^T\right)^{-1}\mathbf{y}, \tag{6}$$

$$\Sigma_x = \left(\Sigma_0^{-1} + \frac{1}{\varepsilon}\Phi^T\Phi\right)^{-1}. \tag{7}$$

The unknown parameters $\varepsilon, \{\gamma_i, \mathbf{B}_i\}_{i=1}^g$ are estimated by a Type II maximum likelihood procedure [22]. After the parameters are estimated, the maximum-a-posteriori (MAP) estimation of $\mathbf{x}$ can be derived directly by $\hat{\mathbf{x}} = \boldsymbol{\mu}_x$ as in (6). The framework above is defined as the BSBL framework [20].

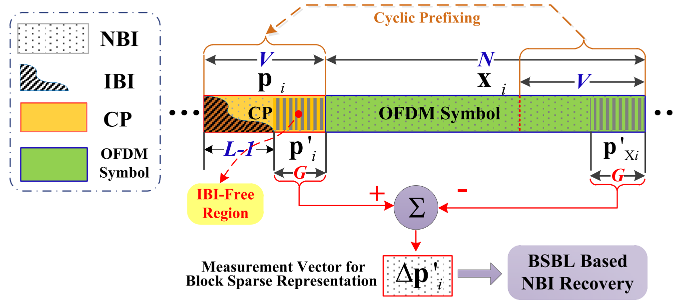

Fig. 1. Block sparse representation for BSBL based NBI recovery through TDM method for CP-OFDM symbol in LTE-A systems.

In our work, the proposed BSBL based algorithm contains the learning rules for the parameters $\varepsilon, \{\gamma_i, \mathbf{B}_i\}_{i=1}^g$. For the first proposed method PE-BSBL, different IBC matrices $\{\mathbf{B}_i\}_{i=1}^g$ are estimated through the learning process. As for the second proposed method I-BSBL, the same IBC matrix is calculated beforehand using the FO matrix, and adopted as an informative aid, which is described in detail in Section IV.

III. System Model

A. CP-OFDM Signal Model in LTE-A

As adopted in LTE-A standards [1], [2] as well as many other broadband transmission systems, the CP-OFDM frame structure is composed of the length-V CP and the length-N OFDM block, as illustrated in Fig. 1. The parameter N is the number of sub-carriers, and the CP part is the last V samples of its following OFDM block. After being transmitted in the wireless multi-path fading channel with the channel impulse response (CIR) $\mathbf{h}_i = \left[h_{i,0}, h_{i,1}, \cdots, h_{i,L-1}\right]^T$ in the presence of NBI generated by NB-IoT signal, the received i-th CP $\mathbf{p}_i = \left[p_{i,0}, p_{i,1}, \cdots, p_{i,V-1}\right]^T$ before the i-th received OFDM block $\mathbf{x}_i$ in the LTE-A system is given by

$$\mathbf{p}_i = \Psi_{\mathrm{CP}}\mathbf{h}_i + \mathbf{e}_i + \mathbf{w}_i, \tag{8}$$

where $\mathbf{e}_i = \left[e_{i,0}, e_{i,1}, \cdots, e_{i,V-1}\right]^T$ denotes the time-domain NBI vector when we look at the CP part, and $\mathbf{w}_i$ denotes the additive white Gaussian noise (AWGN) vector with zero mean and variance of σ_w^2, while the CP component at the receiver is denoted by $\Psi_{\mathrm{CP}}\mathbf{h}_i$, with the matrix $\Psi_{\mathrm{CP}} \in \mathbb{C}^{V \times L}$ given by

$$\begin{bmatrix}
x_{i,N-V} & x_{i-1,N-1} & x_{i-1,N-2} & \cdots & x_{i-1,N-L+1} \\
x_{i,N-V+1} & x_{i,N-V} & x_{i-1,N-1} & \cdots & x_{i-1,N-L+2} \\
x_{i,N-V+2} & x_{i,N-V+1} & x_{i,N-V} & \cdots & x_{i-1,N-L+3} \\
\vdots & \vdots & \vdots & \ddots & \vdots \\
x_{i,N-V+L-2} & x_{i,N-V+L-3} & x_{i,N-V+L-4} & \cdots & x_{i-1,N-1} \\
x_{i,N-V+L-1} & x_{i,N-V+L-2} & x_{i,N-V+L-3} & \cdots & x_{i,N-V} \\
x_{i,N-V+L} & x_{i,N-V+L-1} & x_{i,N-V+L-2} & \cdots & x_{i,N-V+1} \\
\vdots & \vdots & \vdots & \ddots & \vdots \\
x_{i,N-1} & x_{i,N-2} & x_{i,N-3} & \cdots & x_{i,N-L}
\end{bmatrix}$$

whose entries $\{x_{i-1,n}\}_{n=N-L+1}^{N-1}$ represent the last $L-1$ samples of the $(i-1)$-th OFDM block $\mathbf{x}_{i-1}$, which causes inter-block-interference (IBI) on the current i-th CP.

Since the $(i-1)$-th OFDM block $\mathbf{x}_{i-1}$ only causes IBI on the first $L-1$ samples of the i-th CP, the last $G = V - L + 1$ samples of $\mathbf{p}_i$ will form the IBI-free region $\mathbf{p}_i^{'} = \left[p_{i,L-1}, p_{i,L}, \cdots, p_{i,V-1}\right]^T$, i.e., $\mathbf{p}_i^{'} = \mathbf{S}_{G,V}\mathbf{p}_i$, where $\mathbf{S}_{G,V}$ denotes the selection matrix composed of the last G rows of the $V \times V$ identity matrix $\mathbf{I}_V$.

The IBI-free region exists in practical broadband transmission systems because a common rule for system design is to configure the guard interval length V to be much larger than the maximum channel delay spread L in the worst case to avoid IBI between OFDM symbols, so L is usually smaller than V in practice, i.e., $L < V$. For instance, all the IEEE 802.11n [3], the ITU-T G.hn [23], and the 3GPP LTE-A [1] standards based on CP-OFDM obey this rule. Even if in certain extreme cases when the channel delay spread is too long so that it exceeds the guard interval length, the guard interval can be extended to a longer mode to ensure the existence of IBI-free region, which is supported by various standards that have extendable CP length modes [1], [3]. Hence, the IBI-free region at the end of the i-th CP can be rewritten as

$$\mathbf{p}_i^{'} = \Psi_{\mathrm{CP}}^{'}\mathbf{h}_i + \mathbf{e}_i^{'} + \mathbf{w}_i^{'}, \tag{9}$$

where $\mathbf{p}_i^{'}$, $\mathbf{e}_i^{'}$, and $\mathbf{w}_i^{'}$ consist of the last G entries of $\mathbf{p}_i$, $\mathbf{e}_i$, and $\mathbf{w}_i$ in (8), respectively, while $\Psi_{\mathrm{CP}}^{'} \in \mathbb{C}^{G\times L}$ is composed of the last G rows of Ψ_{CP} and contains only the entries in $\mathbf{x}_i$, i.e., $\Psi_{\mathrm{CP}}^{'} = \mathbf{S}_{G,V}\Psi_{\mathrm{CP}}$. The duplicate of $\mathbf{p}_i^{'}$ at the end of the i-th OFDM block $\mathbf{x}_i$ is given by

$$\mathbf{p}_{\mathrm{X}i}^{'} = \Psi_{\mathrm{CP}}^{'}\mathbf{h}_i + \mathbf{e}_{\mathrm{X}i}^{'} + \mathbf{w}_{\mathrm{X}i}^{'}, \tag{10}$$

where $\mathbf{e}_{\mathrm{X}i}^{'}$ and $\mathbf{w}_{\mathrm{X}i}^{'}$ denote the length-G time-domain NBI and AWGN at the end of the i-th OFDM block, respectively.

B. The Block Sparse NBI Model

The NB-IoT signal working in-band in the LTE-A spectrum generates NBI to the receivers of LTE-A systems. In the frequency domain at the receiver in LTE-A systems, the generated NBI associated with the i-th received OFDM block or its CP part is commonly modeled by a superposition of tone interferers represented by a purely sparse vector $\tilde{\mathbf{e}}_i = \left[\tilde{e}_{i,0}, \tilde{e}_{i,1}, \cdots, \tilde{e}_{i,N-1}\right]^T$ with length N, where each tone interferer is a bandlimited Gaussian noise (BLGN) with its central frequency randomly distributed at all the N sub-carriers [24], [25], and the power spectral density (PSD) of $N_{0,\mathrm{NBI}} = \sigma_e^2$. Hence, the spectral amplitude of each tone interferer is a random Gaussian variable with the variance equal to the PSD of the BLGN σ_e^2, and different tone interferers are mutually independent [24]. Accordingly, the time-domain NBI signal $\mathbf{e}_i = [e_{i,0}, e_{i,1}, \cdots, e_{i,V-1}]^T$ associated with the CP as in (8) is given by

$$e_{i,n} = \sum_{k\in\Omega_i} \tilde{e}_{i,k} \cdot \exp\left(\frac{j2\pi kn}{N}\right), \quad n = 0, 1, \cdots, V-1, \tag{11}$$

where $\Omega_i = \left\{k \,\middle|\, \tilde{e}_{i,k} \neq 0\,, k = 0, 1, \cdots, N-1\right\}$ is the set of the locations of nonzero entries, which is defined as the *support*, and the support is assumed to be randomly distributed in all the N sub-carriers. The sparsity level K is defined by the number of nonzero entries, which is much smaller than the signal dimension, i.e. $K = |\Omega_i| \ll N$. The NBI intensity is indicated by interference-to-noise ratio (INR) defined by $\mathbb{E}\{\mathscr{P}_e\}/\sigma_w^2$, with the average power $\mathscr{P}_e = \sum_{k\in\Omega_i} |\tilde{e}_{i,k}|^2/K$ and the variance of the background AWGN σ_w^2. It can be derived that $\mathbb{E}\{\mathscr{P}_e\} = \sigma_e^2$ according to the spectral amplitude distribution, and thus the INR is σ_e^2/σ_w^2.

In practice, the spectral tone interferers of the NBI introduced by the NB-IoT signal might not necessarily locate exactly at the OFDM sub-carriers of the LTE-A system, which extends our NBI model to a more general one [8]. In case there is an FO between the OFDM sub-carriers (i.e. the DFT grid of the LTE-A system) and the NBI (i.e. the NB-IoT frequency locations), each nonzero entry of the purely sparse NBI vector will spread out to a few adjacent sub-carriers, making the frequency domain NBI vector of the i-th CP become a *block sparse* vector $\tilde{\mathbf{e}}_{\mathrm{B}i} = [\tilde{e}_{\mathrm{B}i,0}, \tilde{e}_{\mathrm{B}i,1}, \cdots, \tilde{e}_{\mathrm{B}i,N-1}]^T$ given by

$$\tilde{\mathbf{e}}_{\mathrm{B}i} = \underbrace{\mathbf{F}_N^H \Lambda_{\mathrm{FO}} \mathbf{F}_N}_{\mathbf{C}_{\mathrm{FO}}} \tilde{\mathbf{e}}_i, \tag{12}$$

where $\tilde{\mathbf{e}}_i$ is the purely sparse vector with few nonzero entries, and $\Lambda_{\mathrm{FO}} = \mathrm{diag}\{1, \exp(j2\pi\alpha/N), \cdots, \exp(j2\pi\alpha(N-1)/N)\}$ is the FO matrix with the FO modeled by a uniformly distributed variable $\alpha \in (-1/2, 1/2]$ [8]. Thus the time-domain NBI vector associated with the IBI-free region of the i-th CP in (9) is

$$\mathbf{e}_i^{'} = \mathbf{S}_{G,N}\mathbf{F}_N\tilde{\mathbf{e}}_{\mathrm{B}i}, \tag{13}$$

where $\mathbf{S}_{G,N}$ denotes the selection matrix composed of the last G rows of the $N\times N$ identity matrix $\mathbf{I}_N$, and the last G rows of $\mathbf{F}_N$ is thus denoted by $\mathbf{S}_{G,N}\mathbf{F}_N$. The matrix $\mathbf{C}_{\mathrm{FO}}$ is a *circulant* matrix whose first column is the IDFT of the diagonal of Λ_{FO}. Actually, the purely sparse NBI vector $\tilde{\mathbf{e}}_i$ is a special case of (12) when there is no FO, and we can derive that $\tilde{\mathbf{e}}_{\mathrm{B}i} = \tilde{\mathbf{e}}_i$ and $\mathbf{C}_{\mathrm{FO}} = \mathbf{I}_N$ when $\alpha = 0$. If $\alpha \neq 0$, $\mathbf{C}_{\mathrm{FO}}$ will have a certain number of nonzero entries with significant magnitude at each column. Its physical mechanism is that each original nonzero entry (tone interferer) generates a certain range of frequency spread around its central frequency. Then, by multiplying $\mathbf{C}_{\mathrm{FO}}$ to the purely sparse vector $\tilde{\mathbf{e}}_i$, the vector $\tilde{\mathbf{e}}_{\mathrm{B}i}$ becomes block sparse. Each tone interferer of the purely sparse NBI signal will become a clustered block around the center tone interferer, so the actual sparsity level of the block sparse NBI signal with FO will turn larger than the original sparsity level K of the purely sparse vector. Hence, the number of nonzero blocks in (2) will be $K_g = K$.

Without loss of generality, the same FO α is adopted for the tone interferers for simplicity of presentation in this paper. In fact, this model can be easily extended to different frequency offsets for different tone interferers by setting a distinct FO matrix $\mathbf{C}_{\mathrm{FO},i}$ for each nonzero tone interferer $\tilde{e}_{i,k}$ in (12). The phase offset relation described in the following (16) still holds for each tone interferer $\tilde{e}_{i,k}$ with its own FO α_i. By linear superposition of all the tone interferers, the proposed TDM method and the formulated model (18), as well as the BSBL algorithm described in the following Section IV, still hold in the same way. The model of different FO's has been investigated in literature [41], [42], which can also be referred to for reference.

It should be noted that there is an important characteristic of NBI, which facilitates the proposed method for block sparse representation: the *temporal correlation*. The temporal correlation claims that, both the support and the amplitude of the NBI keep invariant over the received OFDM symbol of interest. First, for the support, the NB-IoT signal working in-band in LTE-A spectrum is located fixed in certain frequency locations in the LTE-A spectrum [5], [7], so the support of the NBI caused by NB-IoT signals keep invariant. The NBI signal in other broadband transmission systems generally comes from the licensed radio services (analog radio and TV broadcasting [26], [27]), narrowband wireless services (e.g. Bluetooth [28]), inappropriate spectrum allocation plans of analogue broadcasting [29], amateur radio signals [30], and narrowband electrical devices emissions (microwave ovens, personal computers [31], [32]) that are working at relatively fixed frequencies. Such interference signals are narrowband and transmitted at relatively constant frequencies so that the NBI can also be assumed to hit the same sub-carriers of the OFDM-based wireless transmission system for over several consecutive OFDM symbols.

As for the amplitude, it can be shown by standards and field tests that, the *coherence time* of the NBI signal is typically longer than that of the received broadband OFDM symbol, so that the amplitude of the NBI signal can be regarded as invariant over the OFDM symbol. Typically, according to the field tests and experimental observations in real house/apartments [33], the NBI interferer source signal has a bandwidth of around 50 - 5000 Hz, resulting in a coherence time of around 200 μs - 20 ms. The supportive data are provided in detail by [33], where it is reported that in many cases, during the mains cycle of alternating current (20 ms), the NBI signal is stationary and its levels do not change based on the field test in [33]. As another example, among the frequencies and bands of radio amateur signals in Italy, most of them have the bandwidth of 200, 500 and 2700 Hz, which implies that the NBI generated by radio amateur ingress will be static over 370 μs - 5 ms. Considering about the NBI generated by NB-IoT signals, the typical duration of one NB-IoT symbol is in the range of 90 μs - 350 μs (OFDM/SC-FDMA modulated, with sub-carrier spacing of 3.75kHz/15kHz, including the guard interval) according to the specifications of NB-IoT [5], [7].

Compared with the relatively long duration of the coherence time of the NBI, the existing broadband transmission systems specify transmission frames (OFDM symbols) with much shorter duration. For instance, the longest CP-OFDM symbol duration (including the guard interval and the IFFT period) of the WLAN system specified in the IEEE 802.11n standard [3], is 3.2 μs for the channel spacing of 5 MHz (see [3, Table 18-5] for detail). For the LTE-A signal, the duration of one OFDM symbol (with sub-carrier spacing of 15kHz, including the cyclic prefix) is less than 72 μs according to the LTE-A standards [1], [2]. Therefore, it is shown that the coherence time of NBI is normally longer than that of the OFDM symbol, which implies that the amplitude of NBI can be considered static over the OFDM symbol.

Due to the temporal correlation of the NBI, the support and amplitude of the NBI associated with the CP part and the following OFDM block part are the same, and only their phases are shifted as follows: the time-domain NBI vector associated with the i-th IBI-free region $\mathbf{e}_i^{'}$ should be equal to the time-domain NBI vector $\mathbf{e}_{\mathrm{X}i}^{'}$ associated with the duplicate of the CP in the following OFDM block with only a phase shift, where $\mathbf{e}_{\mathrm{X}i}^{'}$ is given by

$$\mathbf{e}_{\mathrm{X}i}^{'} = \mathbf{S}_{G,N}\mathbf{F}_N\tilde{\mathbf{e}}_{\mathrm{BX}i}. \tag{14}$$

So the frequency domain block sparse NBI vector $\tilde{\mathbf{e}}_{\mathrm{BX}i} = [\tilde{e}_{\mathrm{BX}i,0}, \tilde{e}_{\mathrm{BX}i,1}, \cdots, \tilde{e}_{\mathrm{BX}i,N-1}]^T$ corresponding to the duplicate part in the OFDM block is the phase shifted vector of $\tilde{\mathbf{e}}_{\mathrm{B}i}$ corresponding to the CP part in (12), which is given by

$$\tilde{e}_{\mathrm{BX}i,k} = \tilde{e}_{\mathrm{B}i,k}\exp\left(\frac{j2\pi(k+\alpha)\Delta l_{\mathrm{B}}}{N}\right), \quad k = 0, 1, \cdots, N-1, \tag{15}$$

where the FO α determines the phase to shift, and Δl_{B} is the distance between the i-th CP and its duplicate at the following OFDM block. Note that $\Delta l_{\mathrm{B}} = N$ in this case and we further have $\tilde{e}_{\mathrm{BX}i,k} = \tilde{e}_{\mathrm{B}i,k}\exp(j2\pi\alpha)$, which yields a simple constant proportional relation only determined by α as follows

$$\tilde{\mathbf{e}}_{\mathrm{BX}i} = \exp(j2\pi\alpha)\,\tilde{\mathbf{e}}_{\mathrm{B}i}. \tag{16}$$

IV. BSBL Based Sparse Approximation of NBI for CP-OFDM Incorporated LTE-A Systems

A. Block Sparse Representation of NBI Through TDM

In CP-OFDM frames, as described in Section III, the time-domain NBI vector $\mathbf{e}_i^{'}$ associated with the i-th IBI-free region $\mathbf{p}_i^{'}$ is described in (13), where its frequency domain form is the block sparse vector $\tilde{\mathbf{e}}_{\mathrm{B}i}$ given in (12).

Firstly, we should establish the block sparse representation of the NBI, which can be implemented by the proposed TDM operation on the CP-OFDM frame. As illustrated in Fig. 1, since the i-th CP is the copy of the last V samples of the i-th OFDM block, the measurement vector can be simply obtained by the differential operation between the received IBI-free region $\mathbf{p}_i^{'}$ in (9) and its duplicate $\mathbf{p}_{\mathrm{X}i}^{'}$ in (10) at the end of the OFDM block, which eliminates the cyclic data component $\Phi_{\mathrm{CP}}^{'}\mathbf{h}_i$ and yields the measurement vector

$$\Delta\mathbf{p}_i^{'} = \Delta\mathbf{e}_i^{'} + \Delta\mathbf{w}_i^{'}, \tag{17}$$

where $\Delta\mathbf{e}_i^{'} = \mathbf{e}_i^{'} - \mathbf{e}_{\mathrm{X}i}^{'}$ and $\Delta\mathbf{w}_i^{'} = \mathbf{w}_i^{'} - \mathbf{w}_{\mathrm{X}i}^{'}$. Thus from (13) and (14), we have the block sparse representation of the NBI as

$$\Delta\mathbf{p}_i^{'} = \mathbf{S}_{G,N}\mathbf{F}_N\Delta\tilde{\mathbf{e}}_{\mathrm{B}i} + \Delta\mathbf{w}_i^{'}, \tag{18}$$

where the length-N block sparse vector to be recovered is

$$\Delta\tilde{\mathbf{e}}_{\mathrm{B}i} = \tilde{\mathbf{e}}_{\mathrm{B}i} - \tilde{\mathbf{e}}_{\mathrm{BX}i} = (1-\exp(j2\pi\alpha))\tilde{\mathbf{e}}_{\mathrm{B}i}, \tag{19}$$

whose support and block partition are the same with those of $\tilde{\mathbf{e}}_{\mathrm{B}i}$ given by (12). Using this block sparse representation in (18), $\Delta\tilde{\mathbf{e}}_{\mathrm{B}i}$ can be recovered from the acquired measurement vector $\Delta\mathbf{p}_i^{'}$ in the presence of background AWGN based on the proposed BSBL underlying method PE-BSBL. Afterwards, $\tilde{\mathbf{e}}_{\mathrm{B}i}$ can be calculated by (19) and the NBI $\tilde{\mathbf{e}}_{\mathrm{BX}i}$ associated with the i-th OFDM block can be calculated through (16). Then, the NBI can be directly cancelled out from the information data in the frequency domain just by subtracting $\tilde{\mathbf{e}}_{\mathrm{BX}i}$ from the received frequency-domain OFDM sub-carriers $\mathbf{X}_i$, which is given by

$$\mathbf{X}_i^0 = \mathbf{X}_i - \tilde{\mathbf{e}}_{\mathrm{BX}i}, \tag{20}$$

where $\mathbf{X}_i$ is the DFT of the i-th received OFDM block $\mathbf{x}_i$ as illustrated in Fig. 1, while $\mathbf{X}_i^0$ is the frequency-domain OFDM data block free from the NBI generated by the NB-IoT signal. Thus, the NBI-free OFDM data block can be then used for information demapping and decoding.

B. NBI Recovery Through PE-BSBL

In the typical BSBL framework described in Section II, the block partition of the block sparse vector to be recovered is known [20]. For initialization, the parameters including $\{\gamma_t, \mathbf{B}_t\}$ and the covariance matrix Σ_0 are estimated. Afterwards, they are input to the BSBL iterations such as the EM method, after which the MAP estimation of the block sparse vector can be calculated.

In the proposed PE-BSBL approach, the block partition of the NBI $\tilde{\mathbf{e}}_{\mathrm{B}i}$ will be firstly estimated by power thresholding. The estimated block partition $\mathbf{\Omega}_{\mathrm{B}i}$ associated with the i-th OFDM block can be acquired by

$$\mathbf{\Omega}_{\mathrm{B}i} = \{k \left| |\Delta\tilde{p}_{i,k}^{'}|^2 > \eta_{th},\ k = 0, 1, \cdots, N-1\},\right. \tag{21}$$

where $\Delta\tilde{\mathbf{p}}_i^{'} = \left[\Delta\tilde{p}_{i,0}^{'}, \Delta\tilde{p}_{i,1}^{'}, \cdots, \Delta\tilde{p}_{i,N-1}^{'}\right]$ is the N-point DFT of $\Delta\mathbf{p}_i^{'}$, and the power threshold η_{th} used to determine the estimated block partition is given by

$$\eta_{th} = \frac{\beta}{N}\sum_{k=0}^{N-1}\left|\Delta\tilde{p}_{i,k}^{'}\right|^2, \tag{22}$$

where β is a scaling coefficient that can be configured proportional to the INR in different scenarios, and is empirically given by $\beta = \sqrt{2\sigma_e^2/\sigma_\omega^2}$ as an appropriate choice. Afterwards, every group of consecutive indices in $\mathbf{\Omega}_{\mathrm{B}i}$ are marked as one nonzero block. Those indices not included in $\mathbf{\Omega}_{\mathrm{B}i}$ are labeled as zero blocks. By labeling these blocks, the initial block partition $\Gamma_i = \{S_t\}_{t=1}^g$ is estimated, where each block is an index set given by

$$S_t = \{d_{t-1}+1, d_{t-1}+2, \cdots, d_t\}, \quad t = 1, 2, \cdots, g, \tag{23}$$

where d_t is the size of the t-th block given in (2) and might be different from each other. Then the initial estimation of the support of the purely sparse vector $\tilde{\mathbf{e}}_i$ in (12) can be obtained by picking out the index of the largest entry in each nonzero block

$$\mathbf{\Omega}_i = \left\{k \left| k \in \mathbf{\Omega}_{\mathrm{B}i}, k = \arg\max_{k\in S_t}\{|\Delta\tilde{p}_{i,k}^{'}|\},\ t = 1, 2, \cdots, g\right.\right\}. \tag{24}$$

After estimating the block partition, the parameters that need to be learnt can be firstly initialized. Set $\gamma_t^{(0)} = 0$ for zero blocks and $\gamma_t^{(0)} = 1$ for nonzero blocks. According to the BLGN a priori distribution of the NBI as described in Section III-B, the variance (auto-covariance) matrix of the purely sparse vector $\tilde{\mathbf{e}}_i$ is a diagonal matrix $\mathbf{V}_{\tilde{\mathbf{e}}_i} \in \mathbb{C}^{N\times N}$ with the diagonal entries being $\{\mathbf{V}_{\tilde{\mathbf{e}}_i}\}_{k,k} = \sigma_e^2$ for $k \in \mathbf{\Omega}_i$, and 0 for $k \notin \mathbf{\Omega}_i$, because the tone interferers are mutually uncorrelated. According to (12),(19) and the property of covariance in linear transform, it is derived that

$$\mathbf{V}_{\Delta\tilde{\mathbf{e}}_{\mathrm{B}i}} = |1-\exp(j2\pi\alpha)|^2\mathbf{C}_{\mathrm{FO}}\mathbf{V}_{\tilde{\mathbf{e}}_i}\mathbf{C}_{\mathrm{FO}}^H \triangleq \Sigma_0^{(0)}, \tag{25}$$

where $\Sigma_0^{(0)} \in \mathbb{C}^{N\times N}$ is the initialized priori covariance matrix of $\Delta\tilde{\mathbf{e}}_{\mathrm{B}i}$. From (4), the IBC matrices $\{\mathbf{B}_t\}_{t=1}^g$ can be initialized by

$$\mathbf{B}_t^{(0)} = \Sigma_0^{(0),t}, \quad t = 1, 2, \cdots, g, \tag{26}$$

where $\Sigma_0^{(0),t} \in \mathbb{C}^{d_t\times d_t}$ denotes the corresponding t-th principal diagonal block in $\Sigma_0^{(0)}$. The block sparse NBI signal also has the a priori Gaussian distribution in (25), because the purely sparse NBI tone interferers are assumed to be Gaussian distributed, and the spectral leakage due to the FO is linear operation so the generated block sparse NBI signal is still Gaussian distributed based on the random process theory. The noise variance $\varepsilon^{(0)}$ can be initialized according to the AWGN distribution or simply set to a value approaching zero [20], [34], and $\varepsilon^{(0)}$ will be adjusted more accurately in the BSBL process.

Then, the BSBL iterations are implemented to recover the block sparse NBI $\Delta\tilde{\mathbf{e}}_{\mathrm{B}i}$ using these initialized parameters. The PE-BSBL algorithm is summarized by the pseudo-code in **Algorithm 1**, where $\boldsymbol{\mu}_x^{(k-1),t} \in \mathbb{C}^{d_t}$ is the corresponding t-th block of $\boldsymbol{\mu}_x^{(k-1)}$. The output of **Algorithm 1** is the recovered block sparse NBI $\Delta\tilde{\mathbf{e}}_{\mathrm{B}i}$.

In the PE-BSBL method, it is assumed that the blocks might have different sizes, so the matrices $\{\mathbf{B}_t\}_{t=1}^g$ are different from each other and required to be estimated through the learning iterations. The block partition is also required to be estimated before the learning process. In fact, the spectral leakage due to the same FO for different blocks can be regarded as the same. Making use of this observation, we can derive the same IBC matrix for different blocks from the FO matrix $\mathbf{C}_{\mathrm{FO}}$ containing the same pattern of scaling coefficients, before the learning iterations to facilitate the BSBL method, which is described in detail in the next sub-section. Hence, another BSBL based method, I-BSBL, is proposed, which is capable of further improving the accuracy of NBI recovery without requiring block partition estimation beforehand.

C. I-BSBL for Block Sparse NBI Reconstruction

For the I-BSBL method, there is no need to estimate the block partition beforehand for initialization. On the other hand, importantly, the IBC within each block caused by the FO can be taken good advantage of as an *informative* aid for the I-BSBL algorithm. The blocks are assumed to have identical size u, and the initial IBC matrices $\{\mathbf{B}_t{}^{(0)}\}_{t=1}^g$ are initialized to

Algorithm 1 Partition Estimated Block Sparse Bayesian Learning (PE-BSBL)

Input:

1) Initial IBC parameters $\{\mathbf{B}_t^{(0)}, \gamma_t^{(0)}\}_{t=1}^{g}$
2) Initial priori covariance matrix $\Sigma_0^{(0)}$
3) Initial noise variance $\varepsilon^{(0)}$
4) Measurement vector $\Delta\mathbf{p}_i^{'}$
5) Observation matrix $\Phi \overset{\Delta}{=} \mathbf{S}_{G,N}\mathbf{F}_N$

Initialization:

$\boldsymbol{\mu}_x^{(0)} \leftarrow \Sigma_0^{(0)}\Phi^T\left(\varepsilon^{(0)}\mathbf{I} + \Phi\Sigma_0^{(0)}\Phi^T\right)^{-1}\Delta\mathbf{p}_i^{'}$

$\Sigma_x^{(0)} \leftarrow \left(\Sigma_0^{(0)-1} + \frac{1}{\varepsilon^{(0)}}\Phi^T\Phi\right)^{-1}$

$\Delta\tilde{\mathbf{e}}_{\mathrm{B}i}^{(0)} \leftarrow \boldsymbol{\mu}_x^{(0)},\ \zeta \leftarrow 1\times 10^{-8},\ k \leftarrow 0$

Iterations:

repeat

$k \leftarrow k+1$ {Next iteration}

$\gamma_t^{(k)} \leftarrow \frac{1}{d_t}\mathrm{Tr}\left[\left(\mathbf{B}_t^{(k-1)}\right)^{-1}\left(\Sigma_x^{(k-1),t} + \boldsymbol{\mu}_x^{(k-1),t}\left(\boldsymbol{\mu}_x^{(k-1),t}\right)^T\right)\right]$

$\varepsilon^{(k)} \leftarrow \frac{1}{G}\left[\left\|\Delta\mathbf{p}_i^{'} - \Phi\boldsymbol{\mu}_x^{(k-1)}\right\|_2^2 + \mathrm{Tr}\left(\Sigma_x^{(k-1)}\Phi^H\Phi\right)\right]$

$\mathbf{B}_t^{(k)} \leftarrow \frac{1}{\gamma_t^{(k)}}\left[\Sigma_x^{(k-1),t} + \boldsymbol{\mu}_x^{(k-1),t}\left(\boldsymbol{\mu}_x^{(k-1),t}\right)^T\right]$

$\Sigma_0^{(k)} \leftarrow \mathrm{diag}\left\{\gamma_1^{(k)}\mathbf{B}_1^{(k)}, \gamma_2^{(k)}\mathbf{B}_2^{(k)}, \cdots \gamma_g^{(k)}\mathbf{B}_g^{(k)}\right\}$

$\boldsymbol{\mu}_x^{(k)} \leftarrow \Sigma_0^{(k)}\Phi^H\left(\varepsilon^{(k)}\mathbf{I} + \Phi\Sigma_0^{(k)}\Phi^H\right)^{-1}\Delta\mathbf{p}_i^{'}$

$\Sigma_x^{(k)} \leftarrow \left(\Sigma_0^{(k)-1} + \frac{1}{\varepsilon^{(k)}}\Phi^T\Phi\right)^{-1}$

$\Delta\tilde{\mathbf{e}}_{\mathrm{B}i}^{(k)} \leftarrow \boldsymbol{\mu}_x^{(k)}$ {The k-th MAP estimation}

until

$\left(\frac{1}{N}\left\|\Delta\tilde{\mathbf{e}}_{\mathrm{B}i}^{(k)} - \Delta\tilde{\mathbf{e}}_{\mathrm{B}i}^{(k-1)}\right\|_1 < \zeta \quad \& \quad \left\|\Delta\mathbf{p}_i^{'} - \Phi\Delta\tilde{\mathbf{e}}_{\mathrm{B}i}^{(k)}\right\|_2^2 < \varepsilon^{(k)}\right)$ {Halting condition}

Output:

Recovered block sparse NBI vector $\Delta\tilde{\mathbf{e}}_{\mathrm{B}i} = \Delta\tilde{\mathbf{e}}_{\mathrm{B}i}^{(k)}$

the same matrix $\mathbf{B}^{(0)} \in \mathbb{C}^{u\times u}$, which is more practical since each tone interferer will spread out to the same number of adjacent sub-carriers with the same scaling coefficients due to the same FO. Note that this can also be derived from (12) where the t-th column ($t = 1, \cdots, N$) of the circulant matrix $\mathbf{C}_{\mathrm{FO}}$ has u significant nonzero entries, i.e. scaling coefficients, around the t-th diagonal entry $(\mathbf{C}_{\mathrm{FO}})_{tt}$, and other entries whose powers are smaller than $\rho|(\mathbf{C}_{\mathrm{FO}})_{tt}|^2$ are neglectable, where ρ is the coefficient used to exclude the insignificant entries. According to the BSBL theory, the algorithm process towards learning the parameters are not sensitive to the choice of the block size u [20], although the computational complexity will be reduced if a suitable u is selected by configuring a very small ρ, such as $\rho = 0.01$, to exclude the insignificant entries. Any tone interferer in $\tilde{\mathbf{e}}_i$ will spread out to the same extent to generate a block in $\tilde{\mathbf{e}}_{\mathrm{B}i}$ with the same block size of u located around this tone interferer, and the IBC of different blocks is identical. Exploiting this property, the identical IBC matrix $\mathbf{B}^{(0)}$ can be exactly initialized from the FO matrix $\mathbf{C}_{\mathrm{FO}}$, which is described in detail in the following content.

Firstly, an artificial non-overlapping block-sparse representation of the NBI is built up in order to cope with the unknown block partition. Since the block partition is unknown, the blocks can be located at arbitrary positions and might overlap with each other. There might be in total $N_{\mathrm{B}} \overset{\Delta}{=} N-u+1$ overlapping blocks in $\Delta\tilde{\mathbf{e}}_{\mathrm{B}i}$, and the t-th block starts and ends at the t-th and $(t+u-1)$-th entries, respectively. All the nonzero entries of $\Delta\tilde{\mathbf{e}}_{\mathrm{B}i}$ lie within a subset of these N_{B} blocks. Since the tone interferers of $\tilde{\mathbf{e}}_i$ are BLGN and the operation of (12) is linear, the t-th block follows a multivariate Gaussian distribution with the covariance matrix of $\gamma_t\mathbf{B}_t$, where $\mathbf{B}_t \in \mathbb{C}^{u\times u}$. As described in Section II, the prior of $\Delta\tilde{\mathbf{e}}_{\mathrm{B}i} \sim \mathcal{N}(\mathbf{0}, \Sigma_0)$, but Σ_0 is no longer block diagonal due to the overlapping of blocks. Each $\gamma_t\mathbf{B}_t$ lies along its principal diagonal and might overlap other neighboring $\gamma_j\mathbf{B}_j (t \neq j)$. Hence, the typical BSBL framework described in the PE-BSBL method requires some modifications to be applicable in the I-BSBL method. The covariance matrix Σ_0 is expanded to a non-overlapping block diagonal matrix $\tilde{\Sigma}_0 \in \mathbb{C}^{N_{\mathrm{B}}u\times N_{\mathrm{B}}u}$ given by

$$\tilde{\Sigma}_0 = \mathrm{diag}\{\gamma_1\mathbf{B}_1, \cdots, \gamma_{N_{\mathrm{B}}}\mathbf{B}_{N_{\mathrm{B}}}\}, \tag{27}$$

where $\{\gamma_t\mathbf{B}_t\}_{t=1}^{N_{\mathrm{B}}}$ no longer overlap with each other. Then the block sparse vector $\Delta\tilde{\mathbf{e}}_{\mathrm{B}i}$ can be decomposed as follows

$$\Delta\tilde{\mathbf{e}}_{\mathrm{B}i} = \sum_{t=1}^{N_{\mathrm{B}}}\mathbf{E}_t\mathbf{z}_t, \tag{28}$$

where each non-overlapping block is denoted by $\mathbf{z}_t \in \mathbb{C}^u$, $\mathbb{E}\{\mathbf{z}_t\} = \mathbf{0}$, $\mathbb{E}\{\mathbf{z}_t\mathbf{z}_j{}^T\} = \delta_{tj}\gamma_t\mathbf{B}_t$ ($\delta_{tj} = 1$ for $t = j$, otherwise $\delta_{tj} = 0$), and the equivalent block sparse vector $\mathbf{z} \overset{\Delta}{=} \left[\mathbf{z}_1^T, \cdots \mathbf{z}_{N_{\mathrm{B}}}^T\right]^T \sim \mathcal{N}_z(\mathbf{0}, \tilde{\Sigma}_0)$. $\mathbf{E}_t \in \mathbb{C}^{N\times u}$ is a zero matrix except that its t-th to $(t+u-1)$-th rows are replaced by the identity matrix $\mathbf{I}_u$. Obviously, the block partition of the artificial block-sparse vector $\mathbf{z}$ is trivial and known, since $\mathbf{z}$ is simply composed of N_{B} neighboring blocks with size of u. Now the equivalent I-BSBL framework corresponding to (18) can be established as

$$\Delta\mathbf{p}_i^{'} = \sum_{t=1}^{N_{\mathrm{B}}}\mathbf{S}_{G,N}\mathbf{F}_N\mathbf{E}_t\mathbf{z}_t + \Delta\mathbf{w}^{'} \overset{\Delta}{=} \mathbf{A}\mathbf{z} + \Delta\mathbf{w}^{'}, \tag{29}$$

where $\mathbf{A} \overset{\Delta}{=} \left[\mathbf{A}_1, \cdots \mathbf{A}_{N_{\mathrm{B}}}\right]$ with $\mathbf{A}_t \overset{\Delta}{=} \mathbf{S}_{G,N}\mathbf{F}_N\mathbf{E}_t$. In this way, the block sparse representation for the I-BSBL method is built and is consistent with the typical BSBL framework given in Section II, since the blocks in $\mathbf{z}$ no longer overlap with each other. It is also derived that $\mathbf{z}$ follows a multivariate distribution. Since the block partition of $\mathbf{z}$ is known, the parameters of the distribution can be learnt through the proposed I-BSBL algorithm whose pseudocode is given in **Algorithm 2**.

The parameters in (27) for the I-BSBL model (29) should be initialized to be input into the process of **Algorithm 2**. As has been analyzed, the IBC matrices (covariance matrix of each block) are identical for realistic NBI with FO. The covariance between any pair of entries within a certain block can be calculated by multiplying their corresponding significant entries (scaling coefficients) in the FO matrix $\mathbf{C}_{\mathrm{FO}}$ given

Algorithm 2 Informative Block Sparse Bayesian Learning (I-BSBL)

Input:

1) Informative IBC $\{\mathbf{B}_t^{(0)} = \mathbf{B}^{(0)}, \gamma_t^{(0)} = \gamma^{(0)}\}_{t=1}^{N_\mathrm{B}}$
2) Informative priori covariance matrix $\tilde{\Sigma}_0^{(0)}$
3) Initial noise variance $\varepsilon^{(0)}$
4) Measurement vector $\Delta\mathbf{p}_i^{'}$
5) *Equivalent* observation matrix $\mathbf{A} \triangleq [\mathbf{A}_1, \cdots \mathbf{A}_{N_\mathrm{B}}]$, where $\mathbf{A}_t \triangleq \mathbf{S}_{G,N}\mathbf{F}_N\mathbf{E}_t$

Initialization:

1: $\boldsymbol{\mu}_x^{(0)} \leftarrow \tilde{\Sigma}_0^{(0)}\mathbf{A}^T\left(\varepsilon^{(0)}\mathbf{I} + \mathbf{A}\tilde{\Sigma}_0^{(0)}\mathbf{A}^T\right)^{-1}\Delta\mathbf{p}_i^{'}$

2: $\Sigma_x^{(0)} \leftarrow \left((\tilde{\Sigma}_0^{(0)})^{-1} + \frac{1}{\varepsilon^{(0)}}\mathbf{A}^T\mathbf{A}\right)^{-1}$

3: $\mathbf{z}^{(0)} \leftarrow \boldsymbol{\mu}_x^{(0)},\ \zeta \leftarrow 1 \times 10^{-8},\ k \leftarrow 0$

Iterations:

4: **repeat**

5: $k \leftarrow k+1$ {Next iteration}

6: $\gamma_t^{(k)} \leftarrow \frac{1}{u}\mathrm{Tr}\left[\left(\mathbf{B}^{(0)}\right)^{-1}\left(\Sigma_x^{(k-1),t} + \boldsymbol{\mu}_x^{(k-1),t}\left(\boldsymbol{\mu}_x^{(k-1),t}\right)^T\right)\right]$

7: $\varepsilon^{(k)} \leftarrow \frac{1}{G}\left[\left\|\Delta\mathbf{p}_i^{'} - \mathbf{A}\boldsymbol{\mu}_x^{(k-1)}\right\|_2^2 + \mathrm{Tr}\left(\Sigma_x^{(k-1)}\mathbf{A}^H\mathbf{A}\right)\right]$

8: $\Sigma_0^{(k)} \leftarrow \mathrm{diag}\left\{\gamma_1^{(k)}\mathbf{B}^{(0)}, \gamma_2^{(k)}\mathbf{B}^{(0)}, \cdots \gamma_{N_\mathrm{B}}^{(k)}\mathbf{B}^{(0)}\right\}$

9: $\boldsymbol{\mu}_x^{(k)} \leftarrow \Sigma_0^{(k)}\mathbf{A}^H\left(\varepsilon^{(k)}\mathbf{I} + \mathbf{A}\Sigma_0^{(k)}\mathbf{A}^H\right)^{-1}\Delta\mathbf{p}_i^{'}$

10: $\Sigma_x^{(k)} \leftarrow \left((\Sigma_0^{(k)})^{-1} + \frac{1}{\varepsilon^{(k)}}\mathbf{A}^T\mathbf{A}\right)^{-1}$

11: $\mathbf{z}^{(k)} \leftarrow \boldsymbol{\mu}_x^{(k)}$ {The k-th MAP estimation}

12: **until** $\left(\frac{1}{uN_\mathrm{B}}\left\|\mathbf{z}^{(k)} - \mathbf{z}^{(k-1)}\right\|_1 < \zeta \quad \& \quad \left\|\Delta\mathbf{p}_i^{'} - \mathbf{A}\mathbf{z}^{(k)}\right\|_2^2 < \varepsilon^{(k)}\right)$ {Halting condition}

Output:

Recovered *equivalent* block sparse vector $\mathbf{z} = \mathbf{z}^{(k)}$

by (12). Thus, the IBC matrix $\mathbf{B}^{(0)} \in \mathbb{C}^{u\times u}$ can be accurately initialized as

$$\mathbf{B}^{(0)} = \sigma_e^2[b_1, b_2\cdots, b_u]^H[b_1, b_2\cdots, b_u], \tag{30}$$

where each corresponding significant entry b_j is given by

$$b_j = (\mathbf{C}_\mathrm{FO})_{j\left\lfloor\frac{u+1}{2}\right\rfloor}, \quad j = 1, 2, \cdots, u, \tag{31}$$

where $\lfloor\cdot\rfloor$ is the floor operator. Because any block of the N_B possible blocks might be nonzero or zero blocks with equal probability, it is assumed that $\gamma_t^{(0)} = \gamma^{(0)} = 1/2, t = 1, \cdots, N_\mathrm{B}$ during the initialization phase, and will be updated to asymptotically approaching either 0 or 1 by the I-BSBL algorithm. Thus, it is derived that the non-overlapping covariance matrix (27) is initialized by

$$\tilde{\Sigma}_0^{(0)} = \frac{1}{2}\mathrm{diag}\{\underbrace{\mathbf{B}^{(0)}, \cdots, \mathbf{B}^{(0)}}_{N_\mathrm{B}\ \text{blocks}}\}. \tag{32}$$

Now the I-BSBL model in (29) can be solved by the proposed **Algorithm 2**. By exploiting the informative parameters (the IBC matrix $\mathbf{B}^{(0)}$, the covariance matrix $\tilde{\Sigma}_0^{(0)}$, and γ_t) in the extended equivalent framework given by (29), the equivalent block sparse vector $\mathbf{z}$ will be recovered by **Algorithm 2** after the learning iterations, and thus the NBI $\Delta\tilde{\mathbf{e}}_{\mathrm{B}i}$ is recovered from (28).

D. Final NBI Cancellation From OFDM Symbols

Till now, we have successfully recovered the block sparse NBI vector, from which the NBI vectors located at the OFDM blocks can be derived due to the temporal correlation of the NBI. The block sparse NBI vector $\tilde{\mathbf{e}}_{\mathrm{BX}i}$ given by (16) located at the i-th OFDM block should be calculated for final cancellation. The block sparse differential NBI vector $\Delta\tilde{\mathbf{e}}_{\mathrm{B}i}$ recovered by the proposed PE-BSBL or I-BSBL algorithms can be exploited to derive the block sparse NBI $\tilde{\mathbf{e}}_{\mathrm{B}i}$ located at the i-th CP according to (19) as follows,

$$\tilde{\mathbf{e}}_{\mathrm{B}i} = \frac{1}{1 - \exp(j2\pi\alpha)}\Delta\tilde{\mathbf{e}}_{\mathrm{B}i} \tag{33}$$

Then $\tilde{\mathbf{e}}_{\mathrm{BX}i}$ can be directly acquired from $\tilde{\mathbf{e}}_{\mathrm{B}i}$ using (16). Afterwards, the NBI signal $\tilde{\mathbf{e}}_{\mathrm{BX}i}$ can be completely and accurately cancelled from the received i-th frequency-domain OFDM block $\mathbf{X}_i$ to obtain the NBI-free OFDM block $\mathbf{X}_i^0$, as given by (20). In this way, the receivers in LTE-A systems are free from the interference generated by the in-band working NB-IoT signals.

V. Performance Evaluation and Simulation Results

The performance of computational complexity, the estimation accuracy and the recovery probability for the proposed BSBL underlying NBI cancellation methods in LTE-A systems is evaluated by extensive simulations. The active data OFDM sub-carrier number is $N = 600$ (when the number of resource block is 50 [1]), and the length of each CP is $V = 144$, as specified in the LTE-A standard [1]. The sub-carrier spacing is 15 kHz, so the occupied active data bandwidth is configured as 9.0 MHz [1], leading to a CP duration of 4.68 μs. In this mode of LTE-A, the total number of sub-carriers considering inactive and other ones is 1024, and the total channel bandwidth is 10.0 MHz [1], [2]. The equivalent baseband multipath six-tap channel, ITU-R Vehicular-A channel model [35] in the presence of NBI with FO, which is widely used to emulate the wireless mobile channel, is applied, where the UE receiver velocity of 20 km/h is used to present the typical low-speed mobile channel. The maximum delay spread of the Vehicular-A channel is 2.51 μs, which is equivalent to the channel length $L = 76$, so the size of the IBI-free region is $G = 68$.[1] As described in Section III-B, each tone interferer of the NBI generated by the NB-IoT signal follows a Gaussian distribution. The FO of the NBI is configured a priori known as $\alpha = 0.20$ in the simulations, while it can

[1]In the simulations, the size of IBI-free region can be pre-determined according to the system configuration of frame length and the maximum channel delay spread of the adopted channel. In realistic implementation, the maximum channel delay spread can also be obtained from the a priori knowledge of the channel environment and channel statistics, or from the coarse channel estimation at the receiver.

also be effectively estimated at the receiver through the grid search method [15] in realistic implementation. Since each NB-IoT signal occupies a bandwidth of 200 kHz according to the NB-IoT specifications [5], which is equivalent to 13 sub-carriers in the LTE-A spectrum, the sparsity level of the NBI is assumed to be $K = 13$ in the simulations to emulate one NB-IoT interfering source signal in the LTE-A system. To make the NBI model more general, the support $\mathbf{\Omega}_i$ of the NBI is assumed to follow a uniform distribution $\mathrm{U}[0, N-1]$ among all the N sub-carriers.[2] The turbo code with code rate of 1/3 as well as the 64QAM modulation as specified in LTE-A [1] are adopted. Besides, the NBI recovery performance of the previously proposed CS based methods, including sparsity adaptive matching pursuit (SAMP) [36] and *a priori* aided SAMP (PA-SAMP) [18], are also evaluated using the same wireless system setup and reported for comparison.

A. Performance Evaluation of Computational and Time Complexity

The computational complexity of the proposed algorithms and the state-of-the-art ones are analyzed and compared in this subsection, which mainly concerned with the two aspects of theoretical analysis and numerical simulations.

1) Theoretical Analysis: The computational complexity and the number of iterations for both the proposed BSBL-based and conventional CS-based algorithms are analyzed theoretically. For conventional CS-based algorithms, the SAMP algorithm [Do08] mainly consumes the complexity in the greedy iterations, where the complexity of each iteration mainly lies in two parts, i.e., the inner product between the observation matrix and the residue, and the equivalent least squares problem. The total number of the iterations is K. Hence, the computational complexity of the conventional SAMP algorithm is $\mathcal{O}(G(K+N)K)$, where G, K, and N denote the size of measurements, the sparsity level, and the size of unknown sparse vector, respectively. Since $N > K$ the complexity is equivalent to $\mathcal{O}(GNK)$. The PA-SAMP algorithm contains the complexity of prior information acquisition, which is implemented by FFT operation. The total average number of iterations is reduced to $K - K_0$ where K_0 is the sparsity level of the prior aided partial support. Hence, the total computational complexity of PA-SAMP is $\mathcal{O}\left(G(K+N)(K-K_0) + N\log_2(N)\right)$, which is equivalent to $\mathcal{O}\left(GN(K-K_0) + N\log_2(N)\right)$. It can be observed that, the total complexity of PA-SAMP and SAMP is linear to the sparsity level K.

For both the proposed BSBL-based algorithms, the complexity mainly lies in the initialization and iterations. As for the initialization, PE-BSBL consumed the complexity of $\mathcal{O}\left(G\left(N^2+G\right)\right)$ from Line 1 in **Algorithm 1**, and $\mathcal{O}\left(N^2G\right)$ from Line 2, so the complexity of initialization of PE-BSBL is $\mathcal{O}\left(G\left(N^2+G\right)\right)$. Here typically one has $N > G$. Besides, PE-BSBL also consumes complexity of $\mathcal{O}\left(N^3\right)$ in block partition estimation mainly due to (25). Similarly one can derive that the complexity of initialization of I-BSBL from Line 1, 2 in **Algorithm 2** is $\mathcal{O}(uNG(uN+G))$, where u denotes the size of each equivalent sub-block and one can derive that $\mathcal{O}(N_{\mathrm{B}}) = \mathcal{O}(N)$. Now considering the complexity of each BSBL iteration, the complexity of PE-BSBL mainly comes from Line 6 - 11 in **Algorithm 1**. Note that the size of sub-block t is denoted by d_t, and the number of sub-blocks g is proportional to the purely sparsity level K, and $N > K$. Then, one has the complexity of each line as follows: Line 6 - $\mathcal{O}\left(N^3/K^2\right)$, Line 7 - $\mathcal{O}\left(N^2G\right)$, Line 8 - $\mathcal{O}\left(N^2/K\right)$, Line 10 - $\mathcal{O}\left(G\left(N^2+G\right)\right)$, Line 11 - $\mathcal{O}\left(N^2G\right)$. Therefore, summing them together, the total complexity of each iteration of PE-BSBL is $\mathcal{O}\left(N^3/K^2 + GN^2\right)$. Similarly, one can derive that the total complexity of each iteration of I-BSBL is $\mathcal{O}\left(u^2N^2G\right)$. Hence, one can infer that the complexity of the proposed BSBL-based algorithms have positive correlation with the size of the unknown sparse vector (N), the size of the measurement vector (G), and the size of the equivalent sub-block for I-BSBL (u), and negative correlation with the sparsity level for PE-BSBL (K).

Furthermore, considering the total number of iterations, it is difficult for the BSBL-based algorithms to derive a closed-form expression of the iteration number. According to the state-of-art BSBL theory [20], the halting condition of BSBL iterations is that the residue should be less than a certain given threshold, which might be reached at any iteration irrelevant to the parameters of K, G, N, etc. Besides, the convergence rate of learning is closely related with the initial status, the fitting extent (whether overfitting or not), and the intensity of NBI with respect to background noise (indicated by INR), etc. Thus, there is no explicit theoretical relationship between the total iteration number and the sparsity level, which is different from conventional CS-based algorithms [37]. However, one can effectively and fairly evaluate the average total number of iterations of BSBL-based algorithms through the following numerical results and simulations.

2) Numerical Results and Simulations: The computational and time complexity of the proposed BSBL-based algorithms and the conventional CS-based algorithms are analyzed and compared, with respect to different sparsity levels and different INR.

Firstly, the runtime (i.e. computational speed) of the proposed BSBL-based and conventional CS-based algorithms with different sparsity levels are simulated and compared, which is presented in Fig. 2. The average runtime for each algorithm is calculated by averaging the runtime of 10^3 simulation estimations. The INR is set to 20 dB. It can be observed from Fig. 2 that the runtime of the conventional CS-based algorithms increases approximately linearly with the sparsity level, which indicates that the computational speed degrades heavily with large sparsity levels. On the other hand, the proposed BSBL-based algorithms are much faster. Especially, the runtime of PE-BSBL is decreasing with respect to the sparsity level, and it can be noted that the computational speed of I-BSBL is almost irrelevant to the sparsity level. These simulation results are all consistent with the previous theoretical analysis.

[2]The parameter K represents the sparsity level of the purely sparse NBI vector without FO, and the number of the nonzero blocks in the block sparse NBI signal with FO is $K_g = K$ as described in Section III-B.

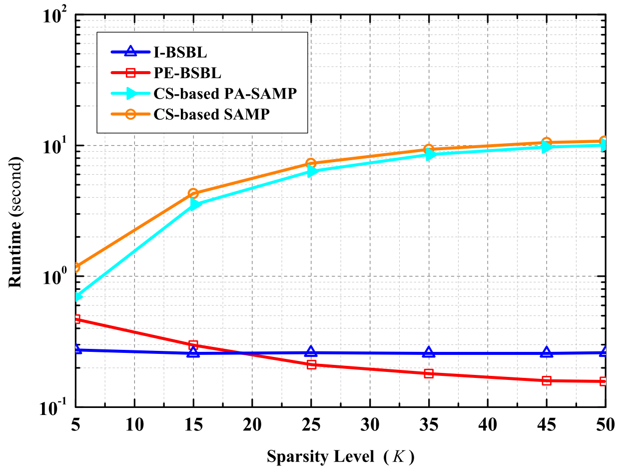

Fig. 2. Comparison of the computational speed of the proposed BSBL-based and conventional CS-based algorithms with respect to sparsity level.

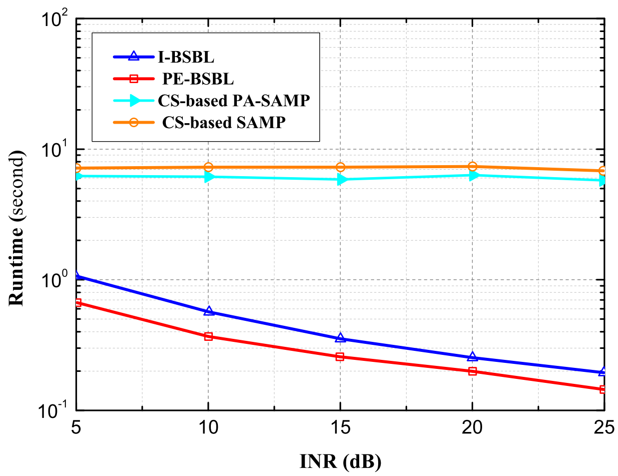

Fig. 3. Comparison of the computational speed of the proposed BSBL-based and conventional CS-based algorithms with respect to INR.

Besides, the runtime the proposed BSBL-based and conventional CS-based algorithms with respect to INR are simulated and compared, which is presented in Fig. 3. The sparsity level is set to $K = 30$. It can be observed from Fig. 3 that the runtime of the conventional CS-based algorithms are significantly higher than the proposed BSBL-based algorithms. Moreover, it is noted that the computational speed of the proposed BSBL-based algorithms increases with the increase of INR, since higher INR leads to the decrease of BSBL learning iterations and faster convergence rate. On the other hand, the runtime of conventional CS-based algorithms keeps invariant because INR has no effect on the number of CS iterations, but just on the MSE performance.

Furthermore, the average number of iterations for the algorithms with respect to sparsity level and INR are numerically analyzed and listed for comparison in Table I and Table II, respectively. The average iteration number of each algorithm is calculated by averaging the iteration number of 10^3 simulation estimations. It is indicated from Table I that the number of iterations for the conventional CS-based algorithms increase linearly with respect to sparsity level, while those of the proposed BSBL-based algorithms almost keep invariant irrelevant

TABLE I

THE AVERAGE NUMBER OF ITERATIONS WITH RESPECT TO SPARSITY LEVEL (INR = 20.0 dB)

Sparsity Level	PA-SAMP	SAMP	PE-BSBL	I-BSBL
10	7.54	9.86	2.18	2.79
20	16.42	20.13	2.24	2.85

TABLE II

THE AVERAGE NUMBER OF ITERATIONS WITH RESPECT TO INR ($K = 30$)

INR (dB)	PA-SAMP	SAMP	PE-BSBL	I-BSBL
10.0	24.71	30.60	6.87	7.10
15.0	24.57	30.42	4.20	4.96

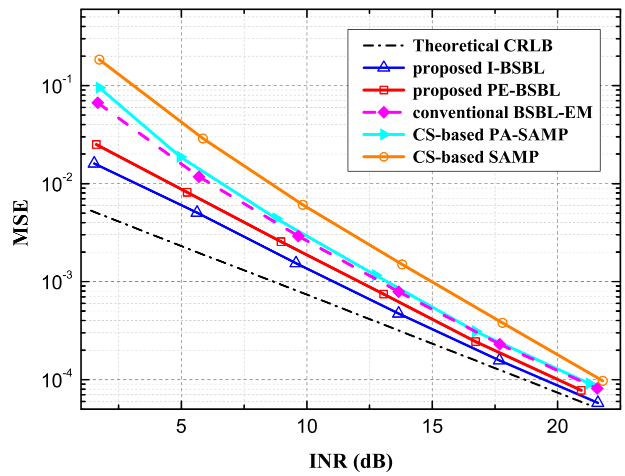

Fig. 4. MSE performance comparisons of the proposed BSBL based method and the CS based counterparts for NBI recovery in the LTE-A system under the wireless Vehicular-A channel.

to the sparsity level, which is consistent with the previous theoretical analysis. From Table II, one can observe that the number of iterations for the conventional CS-based algorithms keep invariant with respect to INR, whereas those of the proposed BSBL-based algorithms decreases with the increase of INR. This is because higher INR will make BSBL iterations converge faster to the precise solution constraint by the halting condition of the BSBL algorithms, which is consistent with the simulation result in Fig.3.

B. Simulation Results and Discussions of NBI Estimation and Cancelation

The mean square error (MSE) performance of NBI recovery using the proposed methods are shown in Fig. 4, with the y-axes being logarithmic. The performances of the proposed BSBL based methods (PE-BSBL and I-BSBL for the recovery of the NBI associated with each CP-OFDM symbol), the conventional BSBL-based algorithm BSBL-EM [20], the CS-based methods (PA-SAMP [18] and SAMP [36] using the preamble to estimate the NBI) are depicted with the sparsity level $K = 13$. The theoretical Cramer-Rao lower bound (CRLB) calculated by $2\sigma_w^2(K/V)$ [18], [38] is also

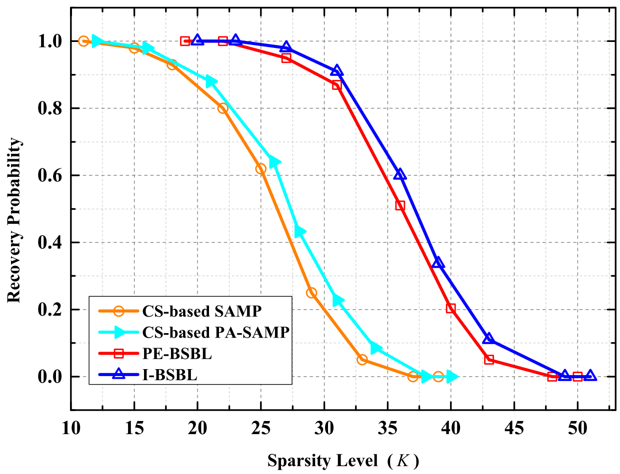

Fig. 5. Probability of NBI recovery using the proposed BSBL and CS based methods in the LTE-A system under the wireless Vehicular-A channel.

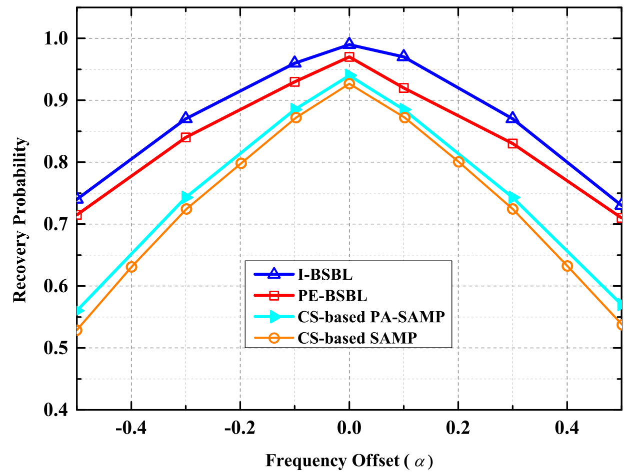

Fig. 6. NBI recovery probability versus different values of FO α in the LTE-A system under the wireless Vehicular-A channel.

included as a benchmark. It is noted from Fig. 4 that the I-BSBL and PE-BSBL methods achieve a target MSE of 10^{-3} at the INR of 11.1 dB and 12.0 dB, respectively, and the I-BSBL approach outperforms the conventional BSBL-based algorithm BSBL-EM, the CS-based algorithms PA-SAMP and SAMP, by approximately 2.0 dB, 2.2 dB and 3.9 dB, respectively. It is also observed that the MSE of the proposed BSBL-based algorithm is asymptotically approaching the theoretical CRLB with the increase of the INR, verifying the validity and accuracy of the proposed methods. The increase of the INR implies that the intensity of the NBI is increased with respect to the background AWGN power, making the NBI signal as measured in the block sparse representation (18) easier to reconstruct, and more accurate.

The recovery probability of the proposed NBI recovery method versus different sparsity levels under the Vehicular-A channel is depicted in Fig. 5 with the INR $=30$ dB and $\alpha=0.2$, with the y-axes being linear. The recovery probability is defined as the rate of the successful NBI estimations (correct support estimation and MSE $<10^{-3}$) to the total estimations. It is noted that the BSBL based methods and the CS based methods reach a successful recovery probability of 0.90 at the sparsity level of $K=31$ and $K=20$, respectively, which indicates that the proposed methods can accurately recover the NBI with large sparsity levels from the acquired measurement data that only has quite a small size. Since each NB-IoT signal occupies 13 sub-carriers in LTE-A spectrum, it is inferred that the proposed BSBL method is capable of effectively recovering and canceling at least 2 in-band NB-IoT interfering signals in the LTE-A system. Moreover, from the gap between the curves of the proposed BSBL and CS based methods, it is implied that the proposed BSBL based methods are more robust to larger sparsity levels, and that the BSBL based methods are particularly effective in recovering the block spare NBI signal that has more nonzero entries due to the spectral spread caused by the FO of the NBI. It can also be noted from Fig. 5 that, CS-based methods cannot reach 100% successful recovery in the presence of 1 NB-IoT interfering signal (corresponding to $K=13$), whereas the proposed BSBL methods have stable 100% successful recovery probability in this case.

To measure the influence of the FO α of the NBI on the proposed methods, the recovery probability versus the FO α under the Vehicular-A channel is illustrated in Fig. 6, where the FO ranges within $\alpha\in(-1/2,1/2]$ and $K=13$ and INR $=30$ dB, with the y-axes being linear. It is noted from Fig. 6 that with the increase of the FO absolute value $|\alpha|$, the recovery successful rate of each method decreases. This trend demonstrates that when there exists a large FO, each tone interferer of the NBI will spread out to more adjacent sub-carriers, resulting in the increase of the sparsity level of the block sparse NBI and causing the degradation of the recovery performance. It is worthwhile to be noted from Fig. 6 that, the proposed I-BSBL and PE-BSBL algorithms significantly outperform the conventional CS-based PA-SAMP and SAMP methods that ignore the IBC within the blocks. With the increase of the FO, each tone interferer spreads out to a wider block, and it is observed that the gain of the proposed BSBL methods over the CS-based methods grows larger. This implies that the two proposed BSBL based methods can fully exploit the IBC within the blocks of the NBI, whereas the CS-based methods cannot. By initializing in advance and iteratively learning the IBC parameters, a more accurate BSBL process is facilitated to achieve a better recovery performance than the CS-based methods. Note that when $\alpha=0$ and the block sparse NBI turns to a purely sparse signal, the BSBL methods still outperform the existing CS-based counterparts, because the purely sparse vector is a special case of block sparse vectors where all block sizes are one, and the *a priori* NBI parameter distribution is fully exploited by the BSBL approach and refined more accurate through learning process.

The bit error rate (BER) performance of the proposed BSBL based methods with INR $=30$ dB and $K=13$ at the UE receiver in the LTE-A system under the wireless Vehicular-A channel is illustrated in Fig. 7, with the y-axes being logarithmic. The LTE-A system configuration is set up according to the parameters given at the beginning of Section V. The BER performances of the conventional

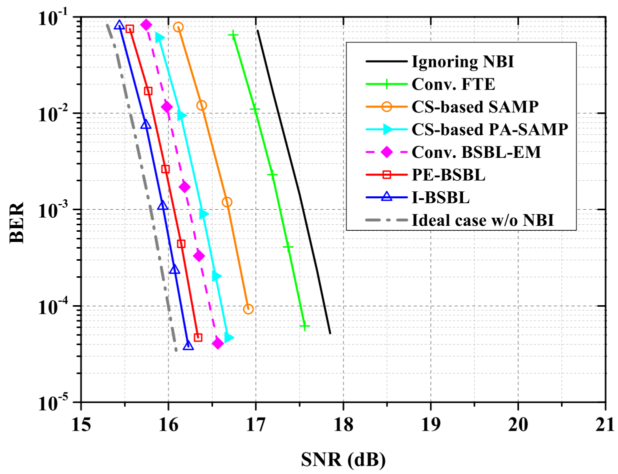

Fig. 7. BER performance comparisons of different NBI mitigation schemes in the LTE-A system under the wireless Vehicular-A channel in the presence of NBI.

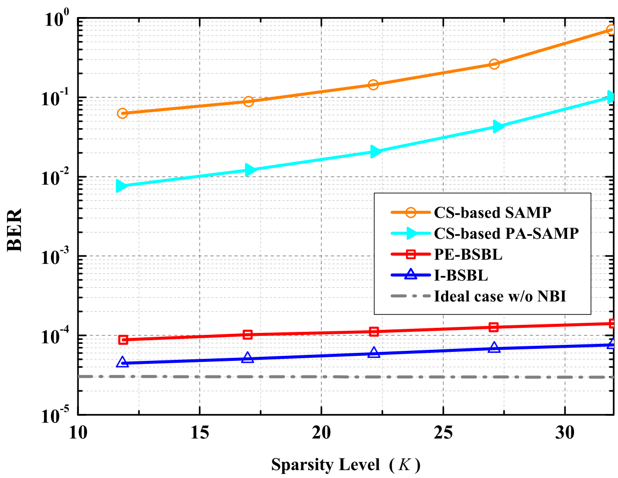

Fig. 8. The BER performance with respect to different sparsity levels under 64QAM.

FTE method [9], the conventional BSBL-based algorithm BSBL-EM [20], and the CS-based methods [18], [36] are presented for comparison. The worst case ignoring NBI and the ideal case without NBI are also depicted as benchmarks. It can be observed that at the target BER of 10^{-4}, the CS methods (SAMP and PA-SAMP) outperform the conventional FTE method and the case ignoring NBI by greater than 0.50 dB and 0.70 dB, respectively. More importantly, it is noted that the proposed BSBL based methods (I-BSBL and PE-BSBL) enjoy a further gain of greater than 0.20 dB and 0.30 dB over the conventional BSBL-based algorithm BSBL-EM and the CS-based methods, respectively, which implies that the IBC within the blocks of the block sparse NBI signal is fully exploited to improve the accuracy and performance of the proposed BSBL algorithm. Furthermore, it is shown in Fig. 7 that the gap between the curves of the proposed I-BSBL method and the ideal case without NBI is only about 0.15 dB, validating the accuracy and effectiveness of the proposed scheme in the wireless transmission environment.

In addition, the BER performance with respect to different sparsity levels under 64QAM at SNR = 16.2 dB is investigated and the result is presented in Fig. 8. It is noted that the BER performance of conventional CS-based algorithms degrades significantly with the increase of sparsity level, whereas the proposed BSBL-based algorithms are hardly influenced. Hence, the proposed BSBL-based algorithms is much more robust to the increase of sparsity level than that of conventional CS-based ones.

VI. Conclusions

The BSBL based framework for NBI cancelation in CP-OFDM-based LTE-A systems has been proposed in this paper. Exploiting the temporal correlation of the NBI generated by NB-IoT signals, the low-complexity TDM method has been proposed to acquire the block sparse representation of the NBI from CP-OFDM frames. A BSBL based method, PE-BSBL, has been proposed to recover the block sparse NBI with FO. By fully exploiting the IBC in the initialization and learning phases, the proposed method was capable of accurately recovering the NBI with FO and large sparsity levels. Making use of the same IBC matrix generated due to the same FO of the NBI, the novel algorithm of I-BSBL has been proposed to further improve the accuracy of NBI recovery. The proposed schemes achieved a much more robust and accurate recovery performance compared with the conventional counterparts, which was validated by extensive simulation results. By effectively canceling the NB-IoT signal interfering the LTE-A system, the UEs in LTE-A systems can operate much more stably and reliably than ever in the presence of in-band working NB-IoT systems, and a harmonic transition and coexistence between 4G and 5G scenarios can be achieved. Furthermore, the proposed BSBL based framework is applicable and can be easily extended to other CP-OFDM based communication systems, which greatly expands the application of the proposed technology.

References

[1] *Evolved Universal Terrestrial Radio Access (E-UTRA); Physical Channels and Modulation (Release 8)*, document 3GPP TS 36.211 v10.3.0, 3GPP ETSI, Sep. 2011.

[2] *Evolved Universal Terrestrial Radio Access (E-UTRA); Base Station (BS) Radio Transmission and Reception (Release 11)*, document 3GPP TS 36.104 v11.4.0, 3GPP ETSI, Apr. 2013.

[3] *Wireless LAN Medium Access Control (MAC) Physical Layer (PHY) Specifications*, IEEE Standard 802.11n, Oct. 2009.

[4] L. Xiao, L. J. Greenstein, N. B. Mandayam, and W. Trappe, "Channel-based spoofing detection in frequency-selective Rayleigh channels," *IEEE Trans. Wireless Commun.*, vol. 8, no. 12, pp. 5948–5956, Dec. 2009.

[5] J. Gozalvez, "New 3GPP standard for IoT," *IEEE Veh. Technol. Mag.*, vol. 11, no. 1, pp. 14–20, Mar. 2016.

[6] J. Meng, "Noise analysis of power-line communications using spread-spectrum modulation," *IEEE Trans. Power Del.*, vol. 22, no. 3, pp. 1470–1476, Jul. 2007.

[7] C. Hoymann *et al.*, "LTE release 14 outlook," *IEEE Commun. Mag.*, vol. 54, no. 6, pp. 44–49, Jun. 2016.

[8] M. S. Sohail, T. Y. Al-Naffouri, and S. N. Al-Ghadhban, "Narrow band interference cancelation in OFDM: A structured maximum likelihood approach," in *Proc. IEEE 13th Int. Workshop Signal Process. Adv. Wireless Commun. (SPAWC)*, Cesme, Turkey, Jun. 2012, pp. 45–49.

[9] K. Shi, Y. Zhou, B. Kelleci, T. W. Fischer, E. Serpedin, and A. L. Karsilayan, "Impacts of narrowband interference on OFDM-UWB receivers: Analysis and mitigation," *IEEE Trans. Signal Process.*, vol. 55, no. 3, pp. 1118–1128, Mar. 2007.

[10] R. Nilsson, F. Sjoberg, and J. P. LeBlanc, "A rank-reduced LMMSE canceller for narrowband interference suppression in OFDM-based systems," *IEEE Trans. Commun.*, vol. 51, no. 12, pp. 2126–2140, Dec. 2003.

[11] D. Darsena, "Successive narrowband interference cancellation for OFDM systems," *IEEE Commun. Lett.*, vol. 11, no. 1, pp. 73–75, Jan. 2007.

[12] D. C. Popescu and P. Yaddanapudi, "Narrowband interference avoidance in OFDM-based UWB communication systems," *IEEE Trans. Commun.*, vol. 55, no. 9, pp. 1667–1673, Sep. 2007.

[13] D. Darsena, G. Gelli, L. Paura, and F. Verde, "A constrained maximum-SINR NBI-resistant receiver for OFDM systems," *IEEE Trans. Signal Process.*, vol. 55, no. 6, pp. 3032–3047, Jun. 2007.

[14] Z. Han, H. Li, and W. Yin, *Compressive Sensing for Wireless Networks*. Cambridge, U.K.: Cambridge Univ. Press, 2013.

[15] A. Gomaa and N. Al-Dhahir, "A sparsity-aware approach for NBI estimation in MIMO-OFDM," *IEEE Trans. Wireless Commun.*, vol. 10, no. 6, pp. 1854–1862, Jun. 2011.

[16] M. Mokhtar, W. U. Bajwa, M. Elgenedy, and N. Al-Dhahir, "Exploiting block sparsity for joint mitigation of asynchronous NBI and IN in hybrid powerline-wireless communications," in *Proc. IEEE Int. Conf. Smart Grid Commun. (SmartGridComm)*, Nov. 2015, pp. 362–367.

[17] H. Al-Tous, I. Barhumi, and N. Al-Dhahir, "Mitigation of narrow-band interference in two-way AF-OFDM relaying systems using compressive sensing," in *Proc. IEEE Wireless Commun. Netw. Conf.*, Apr. 2016, pp. 1–6.

[18] S. Liu, F. Yang, and J. Song, "Narrowband interference cancelation based on priori aided compressive sensing for DTMB systems," *IEEE Trans. Broadcast.*, vol. 61, no. 1, pp. 66–74, Mar. 2015.

[19] S. Liu, F. Yang, W. Ding, X. Wang, and J. Song, "Two-dimensional structured-compressed-sensing-based NBI cancelation exploiting spatial and temporal correlations in MIMO systems," *IEEE Trans. Veh. Technol.*, vol. 65, no. 11, pp. 9020–9028, Nov. 2016.

[20] Z. Zhang and B. D. Rao, "Extension of SBL algorithms for the recovery of block sparse signals with intra-block correlation," *IEEE Trans. Signal Process.*, vol. 61, no. 8, pp. 2009–2015, Apr. 2013.

[21] S. Liu, F. Yang, W. Ding, and J. Song, "NBI cancellation for smart grid communications: A block sparse Bayesian learning perspective," in *Proc. IEEE Int. Conf. Commun. (ICC)*, May 2016, pp. 1–6.

[22] M. E. Tipping, "Sparse Bayesian learning and the relevance vector machine," *J. Mach. Learn. Res.*, vol. 1, pp. 211–244, Jun. 2011.

[23] *Unified High-Speed Wireline-Based Home Networking Transceivers—System Architecture and Physical Layer Specification*, document ITU G.9960, ITU-T, Jun. 2010.

[24] A. M. Tonello and F. Pecile, "Efficient architectures for multiuser FMT systems and application to power line communications," *IEEE Trans. Commun.*, vol. 57, no. 5, pp. 1275–1279, May 2009.

[25] D. Umehara, H. Nishiyori, and Y. Morihiro, "Performance evaluation of CMFB transmultiplexer for broadband power line communications under narrowband interference," in *Proc. IEEE Int. Symp. Power Line Commun. (ISPLC)*, Orlando, FL, USA, Mar. 2006, pp. 50–55.

[26] P. Odling, O. Borjesson, T. Magesacher, and T. Nordstrom, "An approach to analog mitigation of RFI," *IEEE J. Sel. Areas Commun.*, vol. 20, no. 5, pp. 974–986, Jun. 2002.

[27] D. Kang, S. Zhidkov, and H.-J. Choi, "An adaptive detection and suppression of co-channel interference in DVB-T/H system," *IEEE Trans. Consum. Electron.*, vol. 56, no. 3, pp. 1320–1327, Aug. 2010.

[28] J. Park, D. Kim, C. Kang, and D. Hong, "Effect of Bluetooth interference on OFDM-based WLAN," in *Proc. IEEE Veh. Technol. Conf.*, vol. 2. Orlando, FL, USA, Oct. 2003, pp. 786–789.

[29] H. C. Ferreira, L. Lampe, J. Newbury, and T. G. Swart, Eds., *Power Line Communications: Theory and Applications for Narrowband and Broadband Communications over Power Lines*. Chichester, U.K.: Wiley, 2010.

[30] J. Zhang and J. Meng, "Noise resistant OFDM for power-line communication systems," *IEEE Trans. Power Del.*, vol. 25, no. 2, pp. 693–701, Apr. 2010.

[31] Y. Matsumoto, M. Takeuchi, K. Fujii, A. Sugiura, and Y. Yamanaka, "Performance analysis of interference problems involving DSSS WLAN systems and microwave ovens," *IEEE Trans. Electromagn. Compat.*, vol. 47, no. 1, pp. 45–53, Feb. 2005.

[32] Y. Matsumoto, T. Shimizu, T. Murakami, K. Fujii, and A. Sugiura, "Impact of frequency-modulated harmonic noises from PCs on OFDM-based WLAN systems," *IEEE Trans. Electromagn. Compat.*, vol. 49, no. 2, pp. 455–462, May 2007.

[33] J. A. Cortés, L. Díez, F. J. Cañete, and J. J. Sánchez-Martínez, "Analysis of the indoor broadband power-line noise scenario," *IEEE Trans. Electromagn. Compat.*, vol. 52, no. 4, pp. 849–858, Nov. 2010.

[34] D. L. Donoho, M. Elad, and V. N. Temlyakov, "Stable recovery of sparse overcomplete representations in the presence of noise," *IEEE Trans. Inf. Theory*, vol. 52, no. 1, pp. 6–18, Jan. 2006.

[35] *Guideline for Evaluation of Radio Transmission Technology for IMT-2000*, document Rec. ITU-R M.1225, 1997.

[36] T. T. Do, G. Lu, N. Nguyen, and T. D. Tran, "Sparsity adaptive matching pursuit algorithm for practical compressed sensing," in *Proc. Asilomar Conf. Signals, Syst. Comput.*, Oct. 2008, pp. 581–587.

[37] J. A. Tropp and A. C. Gilbert, "Signal recovery from random measurements via orthogonal matching pursuit," *IEEE Trans. Inf. Theory*, vol. 53, no. 12, pp. 4655–4666, Dec. 2007.

[38] S. M. Kay, *Fundamentals of Statistical Signal Processing: Estimation Theory*, vol. 1. Englewood Cliffs, NJ, USA: Prentice-Hall, 1993.

Sicong Liu (S'15) received the B.S.E. degree in electronic engineering from the Department of Electronic Engineering, Tsinghua University, Beijing, China, where he is currently pursuing the Ph.D. degree in electronic engineering with the DTV Technology R&D Center.

His research interests include power line communications, next generation wireless communications, broadband transmission techniques, and interference mitigation.

Fang Yang (M'11–SM'13) received the B.S.E. and Ph.D. degrees in electronic engineering from Tsinghua University, Beijing China, in 2005 and 2009, respectively.

He is currently an Associate Professor with the DTV Technology R&D Center, Tsinghua University. His research interests lie in the field of power line communication, visible light communication, and digital television terrestrial broadcasting.

Jian Song (M'06–SM'10–F'16) received the B.Eng. and Ph.D. degrees in electrical engineering from Tsinghua University, Beijing, China, in 1990 and 1995, respectively. He was with Tsinghua University after graduation, then was with The Chinese University of Hong Kong and the University of Waterloo, Canada, in 1996 and 1997, respectively. He was with Hughes Network Systems, USA, then joined the Faculty Team, Tsinghua University, in 2005 as a Professor. He is currently the Director of Tsinghua's DTV Technology R&D Center. He has been involved in various areas of fiber-optic, satellite and wireless communications, as well as power line communications. His current research interest is in the area of digital TV broadcasting.

He has authored or co-authored over 200 peer-reviewed journal and conference papers. He holds two U.S. and over 40 Chinese patents. He is a fellow of IET.

Zhu Han (S'01–M'04–SM'09–F'14) received the B.S. degree in electronic engineering from Tsinghua University in 1997, and the M.S. and Ph.D. degrees in electrical and computer engineering from the University of Maryland at College Park, College Park, in 1999 and 2003, respectively.

From 2000 to 2002, he was a Research and Development Engineer of JDSU, Germantown, MD, USA. From 2003 to 2006, he was a Research Associate with the University of Maryland. From 2006 to 2008, he was an Assistant Professor with Boise State University, Idaho. He is currently a Professor with the Electrical and Computer Engineering Department as well as with the Computer Science Department, University of Houston, TX, USA. His research interests include wireless resource allocation and management, wireless communications and networking, game theory, big data analysis, security, and smart grid. He was a recipient of an NSF Career Award in 2010, the Fred W. Ellersick Prize of the IEEE Communication Society in 2011, the EURASIP Best Paper Award for the *Journal on Advances in Signal Processing* in 2015, the IEEE Leonard G. Abraham Prize in the field of Communications Systems (the Best Paper Award in the IEEE JOURNAL ON SELECTED AREAS IN COMMUNICATIONS) in 2016, and several best paper awards in the IEEE conferences. He is currently an IEEE Communications Society Distinguished Lecturer.